# Synthesis and Oxygen Release/Storage Properties of Ce-Substituted La-Oxysulfates, $(La_{1-x}Ce_x)_2O_2SO_4$

Dongjie Zhang, Fumihiko Yoshioka, Keita Ikeue, and Masato Machida*

*Department of Nano Science and Technology, Graduate School of Science and Technology, Kumamoto University, 2-39-1 Kurokami, Kumamoto 860-8555, Japan*

*Received June 17, 2008. Revised Manuscript Received August 21, 2008*

A novel oxygen storage material consisting of Ce-substituted La-oxysulfate, $(La_{1-x}Ce_x)_2O_2SO_4$ ($0 \le x \le 0.2$), was synthesized via a surfactant-assisted route. The layered mesophase templated by dodecyl sulfate anion ($DS = C_{12}H_{25}OSO_3^-$) was precipitated from aqueous solutions of nitrates using ammonia as a precipitant. Calcination at ≥500 °C in air yielded the oxysulfate having the monoclinic structure, the lattice constant, *b*, of which was decreased with an increase of the Ce content (*x*) consistent with the smaller ionic radius of $Ce^{3+}/Ce^{4+}$ compared to that of $La^{3+}$. Although part of Ce was deposited as $CeOSO_4$ and/or $CeO_2$ on the oxysulfate, subsequent reduction in $H_2$ yielded single phases of Ce-substituted oxysulfides, $(La_{1-x}Ce_x)_2O_2S$, without forming impurity phases. Easier substitution of La by Ce in oxysulfide than oxysulfate could be confirmed by larger changes of lattice constants, *a* and *c*, for the rhombohedral cell. Sulfur K-edge EXAFS and IR suggested the Ce substitution probably gained distortion of the tetrahedral $SO_4$ unit of $La_2O_2SO_4$. The introduction of Ce in the structure promoted the reduction/reoxidation between oxysulfate and oxysulfide to achieve 4−8 times higher rate of oxygen release/storage. XPS analysis on the solid surface demonstrated that Ce was in the form of $Ce^{3+}/Ce^{4+}$ not only in oxysulfates but also in oxysulfides. The $Ce^{3+}/Ce^{4+}$ species on the surface are therefore considered to facilitate the reduction/reoxidation of sulfur. The resulting smooth oxygen release/storage of $(La_{1-x}Ce_x)_2O_2SO_4$ enhanced the catalytic activity for anaerobic CO oxidation at 600 °C under the unsteady cycled feed stream conditions, where the activity of unsubstituted $La_2O_2SO_4$ was negligible.

## Introduction

So-called oxygen storage materials have become very important in current automotive emission control catalysts.[1−3] Their function is to store or release oxygen in the autoexhaust to achieve the ideal air-to-fuel ratio needed for complete conversion of noxious pollutants including NOx, CO, and hydrocarbons over noble metal catalysts (Pt, Rh, and/or Pd). Conventionally, cerium-based oxides, $CeO_2-ZrO_2$, have been most widely used for this purpose.[4−10] On the basis of redox between $Ce^{4+}$ and $Ce^{3+}$, the oxygen storage capacity (OSC) of 0.25 mol-$O_2$·(mol-Ce)$^{-1}$ is possible. Recently, we have found novel oxygen storage materials, lanthanide oxysulfates ($Ln_2O_2SO_4$), which utilize sulfur as a redox center instead of metallic cations to achieve eight times more OSC, 2 mol-$O_2$·(mol-S)$^{-1}$, than $CeO_2-ZrO_2$ in accordance with the following reaction:[11−16]

$$Ln_2O_2SO_4 \leftrightarrow Ln_2O_2S + 2O_2$$

One drawback of the oxysulfates is their higher operation temperatures ≥600 °C, compared to 300−400 °C required for the $CeO_2-ZrO_2$ system. To overcome this problem, a series of research has been directed toward the microstructural and chemical modifications. Porous structure prepared by a surfactant-templating route increased the specific surface area and the rate of oxygen release/storage.[13] Impregnation of noble metals such as Pt and Pd can also promote the reaction with reducing as well as oxidizing agents.[14] From a material points of view, Ln dependence of oxygen release/storage property is important. Among the series of thermostable $Ln_2O_2SO_4$ (Ln = La, Pr, Nd, and Sm), the Pr compound can work at the lowest possible temperature, because $Pr^{3+}/Pr^{4+}$ species on the surface play a role of mediator for the redox of sulfur.[15,16] In addition, structural

* Corresponding author. E-mail: machida@chem.kumamoto-u.ac.jp.

(1) Taylar, K. C. Automobile catalytic converters. In *Catalysis-Science and Technology*; Anderson, J. R., Boudart, M., Eds.; Springer-Verlag: Berlin, 1984; Vol. 5.
(2) Bernal, S.; Kaspar, J.; Trovarelli, A. *Catal. Today* **1999**, *2*, 50.
(3) Trovarelli, A. *Catalysis by ceria and related materials*; Trovarelli, A., Ed.; Imperial College Press: London, 2002; Vol. 2.
(4) Ozawa, M; M. Kimura, M.; Isogai, A. *J. Alloys Compd.* **1993**, *193*, 73.
(5) Zamur, F.; Trovarelli, A.; de Leitenburg, C.; Dolcetti, G. *J. Chem. Soc., Chem. Commun.* **1995**, 965.
(6) Balducci, G.; Fornasiero, P.; Di Monte, R.; Kaspar, J.; Meriani, S.; Graziani, M. *Catal. Lett.* **1995**, *33*, 193.
(7) Kaspar, J.; Fornasiero, P. *J. Solid State Chem.* **2003**, *171*, 19.
(8) Pijolat, M.; Prin, M.; Soustelle, M.; Touret, O.; Nortier, P. *J. Chem. Soc., Faraday Trans.* **1995**, *91*, 3941.
(9) Dutta, G.; Waghmare, U. V.; Baidya, T.; Hegde, M. S.; Priolkar, K. R.; Sarode, P. R. *Chem. Mater.* **2006**, *18*, 3249.
(10) Imanaka, N.; Masui, T.; Minami, K.; Koyabu, K. *Chem. Mater.* **2005**, *17*, 6511.
(11) Machida, M.; Kawamura, K.; Ito, K. *Chem. Commun.* **2004**, 662.
(12) Machida, M.; Kawamura, K.; Ito, K.; Ikeue, K. *Chem. Mater.* **2005**, *17*, 1487.
(13) Machida, M.; Kawamura, K.; Kawano, T.; Zhang, D.; Ikeue, K. *J. Mater. Chem.* **2006**, *16*, 3084.
(14) Ikeue, K.; Eto, M.; Zhang, D.; Kawano, T.; Machida, M. *J. Catal.* **2007**, *248*, 46.
(15) Machida, M.; Kawano, T.; Eto, M.; Zhang, D.; Ikeue, K. *Chem. Mater.* **2007**, *19*, 945.
(16) Ikeue, K.; Kawano, T.; Eto, M.; Zhang, D.; Machida, M. *J. Alloys. Compd.* **2008**, *451*, 338.

10.1021/cm801629b CCC: $40.75 
Published on Web 10/15/2008

analysis by means of XRD and IR implies that sulfate reduction becomes easier with increasing distortion of the tetragonal $SO_4$ unit in the oxysulfate.

On the basis of these results, we propose here the concept for the design of Ln−oxysulfate materials, which includes the working hypothesis that oxygen storage can be facilitated (i) by introducing redox species and/or (ii) by increasing distortion of the $SO_4$ unit. With these points taken into consideration, the structural modification by means of partial substitution of Ln has been studied in the present work. Although Ce takes both tetravalent and trivalent states, it cannot form stable oxysulfates.[12,15] La forms most thermostable oxysulfates among the lanthanides, but the lack of redox property of $La^{3+}$ leads to higher working temperature compared to the Pr system. Because Pr is a high cost and less-abundant resource compared to La and Ce, its replacement is of great interest to the practical applications. With the intention of promoting the oxygen release/storage of $La_2O_2SO_4$, Ce-substituted $La_2O_2SO_4$ has been synthesized for the first time by the surfactant-templating method and characterized be means of XRD, XAFS, XPS, and IR. For catalytic application, $(La_{1-x}Ce_x)_2O_2SO_4$ was applied to anaerobic oxidation of CO under cycled feed stream conditions.

## Experimental Section

The Ce-substituted oxysulfates, $(La_{1-x}Ce_x)_2O_2SO_4$ ($x = 0$, 0.1, and 0.2), were synthesized by a template-assisted route as reported in our previous paper.[13] $La(NO_3)_3 \cdot 6H_2O$ (Mitsuwa Chemical, 99.9%), $Ce(NO_3)_3 \cdot 6H_2O$ (Mitsuwa Chemical, 99.9%), $C_{12}H_{25}OSO_3Na$ (SDS, Kishida Chemical, 98.5%), aqueous ammonia, and deionized water in a molar ratio of (La + Ce):SDS:$NH_3$:$H_2O$ = 1:2:30:60 were mixed at 40 °C for 1 h and then kept stirring at 50 °C for 10 h to obtain a uniform layered mesophase ($La_{1-x}Ce_x$-DS). The precipitate was thoroughly washed with deionized water and dried by evacuation overnight. The solid thus obtained was calcined at elevated temperatures in air to obtain $(La_{1-x}Ce_x)_2O_2SO_4$, which can also be transformed into $(La_{1-x}Ce_x)_2O_2S$ by reducing in a flow of $H_2$ at 700 °C. As prepared oxysulfate calcined at 800 °C was impregnated with an aqueous solution of $Pd(NO_3)_2$ and then calcined at 400 °C to produce Pd-loaded samples (1 wt % loading).

The powder XRD was measured on a Rigaku Multiflex diffractometer with monochromated Cu Kα radiation (40 kV, 20 mA). Lattice constants of oxysulfate and oxysulfide were calculated and corrected using a MDI JADE software. Energy-dispersive X-ray fluorescence analysis (Horiba MESA-500W) was used to determine the chemical composition. The BET surface area was calculated from $N_2$ desorption isotherms measured at 77 K (Belsorp). Fourier transform infrared spectra were recorded on Jasco FTIR 610 spectrometer by using a KBr method.

The XPS spectra were measured on a VG Sigmaprobe spectrometer using Al Kα radiation (15 kV, 7 mA). The binding energy calculation was checked using the line position of C 1s as an internal reference. The charging effect was ruled out in the measurement because the binding energy for C 1s was identical for all of the samples. The normal operating pressure in the analysis chamber was controlled at less than $10^{-6}$ Pa during the measurement.

The X-ray absorption spectrum of the S K-edge was recorded on a BL-11B instrument at the Photon Factory (PF) of the High Energy Accelerator Research Organization (KEK) with a ring energy of 2.5 GeV and a stored current of around 300−450 mA. A Ge(111) double-crystal monochromator was used. Spectral recording was performed at room temperature in the total electron/fluorescence electron yield mode. Measurements were carried out in a high-vacuum chamber. A grounded picoammeter was connected to the sample to measure total electron yield as drain current. Another picoammeter was connected to a Ni mesh, which was placed in the synchrotron radiation pathway, to evaluate incident beam intensity. Sample powders were attached to the perpendicular stage using carbon double-sided adhesive tape. The XAFS data were processed using a REX 2000 program (Rigaku). EXAFS oscillation was extracted by fitting a cubic spline function through the postedge region. The $k^3$-weighted EXAFS oscillation in the 3.0−13.0 $Å^{-1}$ regions was Fourier-transformed. Phase shift and backscattering amplitude were obtained from the EXAFS data of $Cs_2SO_4$ for S−O.

**Table 1. Molar Ratio of S/(La + Ce) for $(La_{1-x}Ce_x)_2O_2SO_4$ before and after Calcination at Various Temperatures in Air for 1 h[a]**

| $x$ | as precipitated | 500 °C | 600 °C | 700 °C | 800 °C | 900 °C |
|---|---|---|---|---|---|---|
| 0 | 0.52 | 0.49 | 0.47 | 0.45 | 0.47 | 0.48 |
| 0.1 | 0.49 | 0.53 | 0.48 | 0.52 | 0.45 | 0.32 |
| 0.2 | 0.51 | 0.54 | 0.49 | 0.49 | 0.49 | 0.29 |

[a] Uncertainties in the ratios are ± 0.01.

The oxygen release and storage behavior of 1 wt % Pd/$(La_{1-x}Ce_x)_2O_2SO_4$ was evaluated by the use of the flow microbalance (Rigaku 8120). The change of sample weight (10 mg) was measured during heating at constant rate of 10 °C·$min^{-1}$ in a flow of 1.4% $H_2$/He or 0.7% $O_2$/He. The dynamic reduction−oxidation cycles were also measured in the same system. For this experiment, as-prepared 1 wt % Pd/$(La_{1-x}Ce_x)_2O_2SO_4$ was first heated in a flow of $N_2$ up to 600 °C, where the constant weight was attained within 30 min. Then, the gas feed to the sample was switched at a certain interval between 1.4% $H_2$/He and 0.7% $O_2$/He (70 $cm^3 \cdot min^{-1}$) with recording the sample weight at this temperature.

Anaerobic CO oxidation under cycled feed stream conditions was performed at constant reaction temperatures (400−700 °C) in a dual-supply flow system. Two gas feeds, 1% CO/He and 0.5% $O_2$/He were switched with the programmed time intervals. The rate of the gas feed was controlled at $W/F = 4 \times 10^{-3}$ g·min·$cm^{-3}$. The concentrations of each gas component (CO, $CO_2$, and $O_2$) were recorded before and after the catalyst bed using a quadrupole mass spectrometer (Pfeiffer, Omnistar).

## Results and Discussion

**Crystal Structure of Ce-Substituted Oxysulfates.** Table 1 shows the molar ratio of S/(La + Ce) for the products having nominal compositions of $(La_{1-x}Ce_x)_2O_2SO_4$ ($x = 0$, 0.1, and 0.2) before and after calcination at elevated temperatures in air. As precipitated solids contained the template DS molecule in accordance with the stoichiometry of oxysulfate, S/(La + Ce) = 0.5. In all cases, the content of sodium was negligible. Figure 1 shows the XRD patterns of $La_{0.8}Ce_{0.2}$-DS ($x = 0.2$) before and after calcination in air. Three diffraction peaks at $2\theta \leq 10°$ of the as-prepared precipitate were indexed as the (001), (002), and (003) reflections, suggesting a layered structure with the interlayer distance of 3.68 nm. The other two broad and weak peaks at around $2\theta = 27$ and 56° matched with the $d_{110}$ and $d_{220}$ of $La(OH)_3$, respectively. These observations are consistent with an ordered layered mesophase consisting of alternative stacking of a lanthanide-hydroxide layer ($La_2(OH)_5^+$) and a $DS^-$ bilayer as reported in our previous paper.[13] The interlayer distance (3.68 nm) is therefore rationalized by the

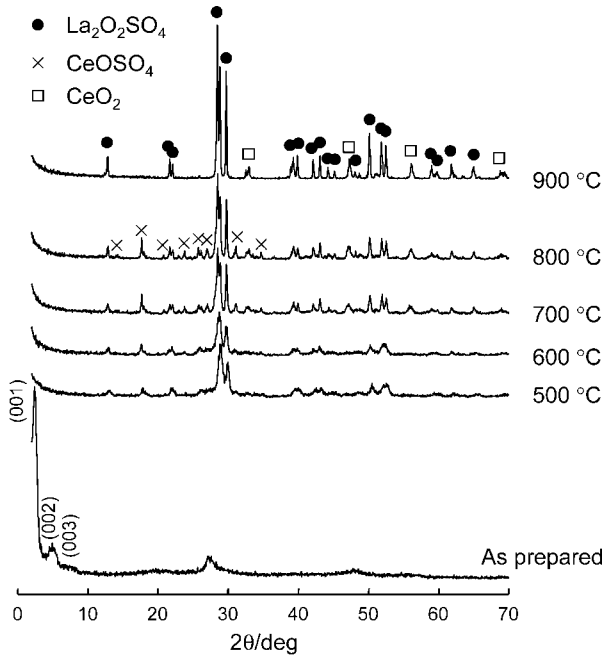


**Figure 1.** XRD patterns of $La_{0.8}Ce_{0.2}$-DS before and after calcination at elevated temperature in air for 1 h.

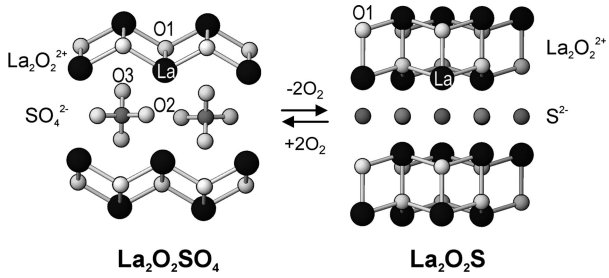


**Figure 2.** Crystal structures of $La_2O_2SO_4$ and $La_2O_2S$.

sum of a $1 \times c_0$ thick La hydroxide layer (0.377 nm) and thickness of DS bilayer tilting by approximately 60° with respect to the La hydroxide layer (3.3 nm). The absence of Ce hydroxide is an indication of that part of the La site in the mesophase is occupied by Ce.

Upon heating the precipitate in air, the layered mesophase was collapsed at 200 °C to yield a noncrystalline phase (Figure 1), but the S/(La + Ce) ratio was kept almost constant at about 0.5. Further calcination at ≥500 °C gave the diffraction pattern, which is assigned to $La_2O_2SO_4$ with the monoclinic structure (*C*2/*c*). The crystal structure of $La_2O_2SO_4$ is described by alternative stacking of a $La_2O_2^{2+}$ layer and a layer of sulfate ($SO_4^{2-}$) as depicted in Figure 2. The $La_2O_2^{2+}$ layer consists of $OLa_4$ tetrahedra linked together by sharing of edges.[17] The lattice parameters of $(La_{1-x}Ce_x)_2O_2SO_4$ after calcination at 800 °C were calculated as shown in Table 2. In contrast to almost constant values of *a* and *c*, the *b* tends to decrease with an increase of *x*. This change is reasonable considering that part of La is replaced by Ce with a smaller ionic radius ($La^{3+}$, 0.120 nm; $Ce^{3+}$, 0.117 nm; and $Ce^{4+}$, 0.094 nm). However, the change of lattice parameters was not observed when the sample was

(17) Zhukov, S.; Yatsenko, A.; Chernyshev, V.; Trunov, V.; Tserkovnaya, E.; Anston, O.; Hosla, J.; Baules, P.; Schenk, H. *Mater. Res. Bull.* **1997**, *32*, 43.

**Table 2. Lattice Parameters of Monoclinic $(La_{1-x}Ce_x)_2O_2SO_4$**

| *x* | *a*, nm | *b*, nm | *c*, nm | *β*, deg |
|---|---|---|---|---|
| 0[a] | 1.4354(3) | 0.42862(6) | 0.8388(2) | 107.16(2) |
| 0.1[a] | 1.4356(2) | 0.42845(4) | 0.8390(1) | 107.06(2) |
| 0.2[a] | 1.4356(3) | 0.42826(8) | 0.8389(2) | 107.05(3) |
| 0[b] | 1.4359(2) | 0.42848(4) | 0.8389(1) | 107.06(1) |
| 0.2[b] | 1.4353(5) | 0.42863(9) | 0.8390(3) | 107.15(3) |

[a] After calcination at 800 °C in air for 1 h. [b] After calcination at 900 °C in air for 1 h.

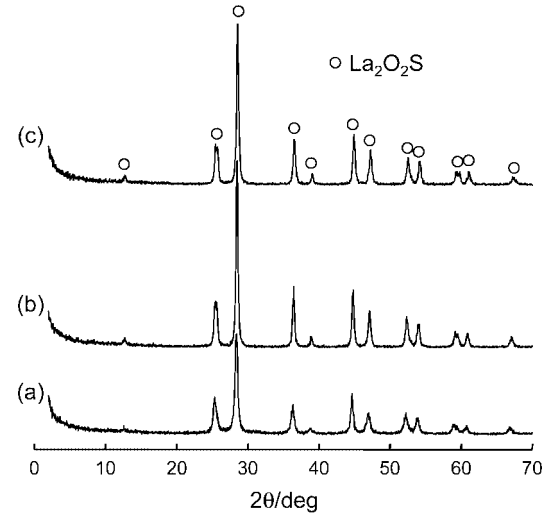


**Figure 3.** XRD patterns of $(La_{1-x}Ce_x)_2O_2S$ with (a) $x = 0$, (b) 0.1, and (c) 0.2 obtained after heating at 700 °C in $H_2$ for 1 h.

calcined at 900 °C, suggesting a large part of Ce in the oxysulfate structure was deposited as $CeO_2$ at this temperature.

As shown in Figure 1, the products obtained at 500−800 °C contained an impurity ascribable to $CeOSO_4$, which was decomposed to yield $CeO_2$ at 900 °C. At this temperature, the diffraction peaks of $La_2O_2SO_4$ were intensified, and simultaneously, the S/(La + Ce) ratio decreased from 0.49 to 0.29 (Table 1), suggesting the following partial decomposition of the oxysulfate.

$$(La_{1-x}Ce_x)_2O_2SO_4 \rightarrow (1-x)La_2O_2SO_4 + 2xCeO_2 + xSO_2$$

Because the observed S/(La + Ce) ratios (0.29 for $x = 0.2$) were smaller than that expected from above reaction (0.4 for $x = 0.2$), further decomposition of $La_2O_2SO_4$ may also be induced in part. These results suggest that the thermostability of oxysulfate is decreased by the Ce-substitution.

When oxysulfates obtained after heating at 800 °C were subsequently reduced in a flow of $H_2$ at 700 °C, the XRD pattern was changed as shown in Figure 3. Unlike the case of oxysulfate, all of the compounds showed the reflections ascribable only to rhombohedral (*P*3*m*1) oxysulfide ($La_2O_2S$), but no impurity phases were detected. As shown in Figure 2, $La_2O_2S$ resembles $La_2O_2SO_4$ in ionic arrangements consisting of a $La_2O_2^{2+}$ layer and a layer of sulfide ($S^{2-}$).[18] Because each diffraction peak in Figure 3 was found to shift to the higher $2\theta$ with an increase of *x*, the lattice parameters of oxysulfide were calculated as shown in Table 3. Clearly, both *a* and *c* decreasing with an increase of *x* convinces the formation of oxysulfide solid solutions, $(La_{1-x}Ce_x)_2O_2S$.

(18) Zachariasen, W. H. *Acta Crystallogr.* **1948**, *1*, 265.

**Table 3. Lattice Parameters of Rhombohedral $(La_{1-x}Ce_x)_2O_2S$**

| $x$ | $a$, nm | $c$, nm |
|---|---|---|
| 0[a] | 0.4054(3) | 0.6927(8) |
| 0.1[a] | 0.4041(2) | 0.6924(4) |
| 0.2[a] | 0.4028(2) | 0.6907(4) |

[a] After calcination at 800 °C in air for 1 h and subsequently at 700 °C in $H_2$ for 1 h.

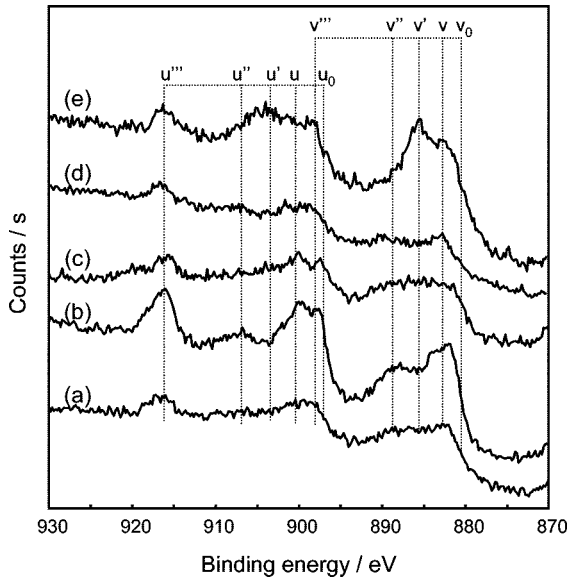


**Figure 4.** Ce 3d spectra of (a) $(La_{0.9}Ce_{0.1})_2O_2SO_4$, (b) $(La_{0.8}Ce_{0.2})_2O_2SO_4$ after calcination in air at 800 °C, (c) $(La_{0.9}Ce_{0.1})_2O_2SO_4$, (d) $(La_{0.8}Ce_{0.2})_2O_2SO_4$ after calcination in air at 900 °C, and (e) $(La_{0.8}Ce_{0.2})O_2S$ after reduction at 800 °C.

These results support that part of Ce seems to replace the La site to form $(La_{1-x}Ce_x)_2O_2SO_4$ at ≤800 °C, although actual Ce content in oxysulfate is less than the nominal value ($x$). It should be noted that such Ce-substituted La-oxysulfates can successfully be synthesized at low temperatures by the present templating route. This is in contrast to a conventional simple coprecipitation method, which requires heating the precursor above 800 °C to decompose sulfate to oxysulfate, but the product was a mixture of $La_2O_2SO_4$ and $CeO_2$. Even in the present synthetic route, a large part of Ce would be deposited as $CeOSO_4$ or $CeO_2$. This is quite different from Ce-substituted $La_2O_2S$ that could be formed as a single phase. A higher capability of Ce substitution for $La_2O_2S$ rather than $La_2O_2SO_4$ can be explained by the valence of Ce, which should be reduced to 3+ in a flow of $H_2$. By contrast, $Ce^{4+}$ formed in an oxidizing atmosphere is difficult to accommodate in the La site of $La_2O_2SO_4$. Consequently, the charge compensation mechanism of the present system cannot be described clearly because of the phase complexity owing to the impurity ($CeO_2SO_4$ and $CeO_2$).

**Oxidation State of Ce.** Figure 4 depicts Ce 3d XPS spectra of $(La_{1-x}Ce_x)_2O_2SO_4$ and $(La_{1-x}Ce_x)_2O_2S$. The Ce 3d spectrum consists of $3d_{5/2}$ and $3d_{3/2}$ peaks and satellite peaks as a result of the hybridization with O 2p orbitals and partial occupation of the 4f levels. It was reported that signals at the binding energies of 882.4 (v), 888.6 (v″), 898.3 (v‴), 901.1 (u), 907.8 (u″), and 916.6 eV (u‴) are assigned to $3d_{5/2}$ and $3d_{3/2}$ characteristic for $Ce^{4+}$, whereas those at 880.8 ($v_0$), 885.7 (v′), 897.4 ($u_0$), and 903.7 eV (u′) are characteristic for $Ce^{3+}$.[19−22] Two $(La_{1-x}Ce_x)_2O_2SO_4$ samples ($x = 0.1$ and 0.2) after heating at 800 °C (a and b) showed that Ce was mainly in the form of $Ce^{4+}$ in contrast to its formal charge in the oxysulfate which is 3+. After heating at 900 °C (c and d), all peaks became less intense with simultaneous deposition of $CeO_2$, but they still showed $Ce^{4+}$ as a primary state. The weakened peaks are associated with $CeO_2$ having a large crystallite size and thus very small surface coverage. On the surface of $(La_{0.8}Ce_{0.2})_2O_2S$ (e), which was obtained by heating in a stream of $H_2$, the signals ascribable to $Ce^{3+}$ appeared, while the $Ce^{4+}$ species still remained. These results suggest that the surfaces of Ce substituted oxysulfates as well as oxysulfides are easily oxidized to yield a considerable amount of $Ce^{4+}$. Because this is very similar to $Pr^{4+}$ species formed on the surface of $Pr_2O_2SO_4/Pr_2O_2S$ in our previous work,[15] the easier formation of tetravalent cations is associated with the oxidation potential of lanthanide elements. Nevertheless, the total concentration of $Pr^{4+}$ was found to be negligible when all of the bulk Pr is taken into consideration. The redox between $Pr^{3+}$ and $Pr^{4+}$ on the surface is one important reason for the highest rate of the oxygen release/storage among the series of $Ln_2O_2SO_4$ (Ln = La, Pr, Nd, and Sm). The charge compensation accompanied by the redox of Pr is considered to cause the adsorption or desorption of oxygen and thus promote the redox of sulfur. Therefore, the redox between $Ce^{3+}$ and $Ce^{4+}$ in the present system is also expected to be effective in accelerating the oxygen release/storage.

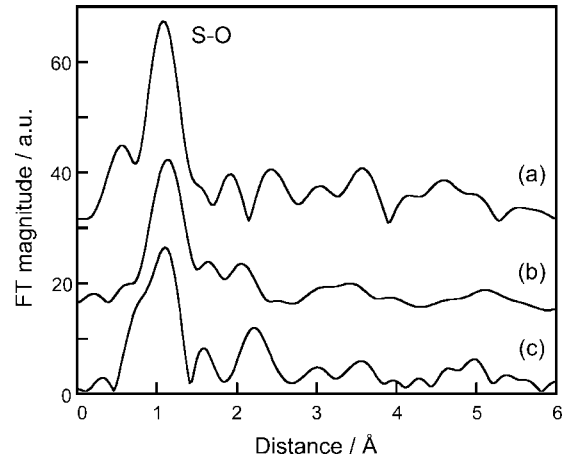


**Figure 5.** Fourier transforms of S K-edge EXAFS for $(La_{0.8}Ce_{0.2})_2O_2SO_4$ after calcination at (a) 800 °C and (b) 900 °C. (c) $La_2O_2SO_4$ as a reference.

**Local Structure of Sulfate.** The local environment of sulfur in $(La_{1-x}Ce_x)_2O_2SO_4$ was analyzed by EXAFS. Figure 5 shows the Fourier transforms of S K-edge EXAFS for $(La_{0.8}Ce_{0.2})_2O_2SO_4$ (a,b) together with that of unsubstituted $La_2O_2SO_4$ (c). These spectra are not corrected for phase shift so that the observed peaks are shifted to lower $r$ values from

(19) Kobayashi, Y.; Fujiwara, Y. *J. Alloys Compd.* **2008**, *1157*, 408–412.
(20) Pozdnyakova, O.; Teschner, D.; Wootsch, A.; Kröhnert, J.; Steinhauer, B.; Sauer, H.; Toth, L.; Jentoft, F. C.; Knop-Gericke, A.; Paál, Z.; Schlögl, R. *J. Catal.* **2006**, *237*, 1.
(21) Pfau, A.; Schierbaum, K. D. *Surf. Sci.* **1994**, *321*, 71.
(22) Sarma, D. D.; Rao, C. N. R. *J. Electron Spectrosc. Relat. Phenom.* **1980**, *20*, 25.

**Table 4. Structural Parameters of $(La_{1-x}Ce_x)_2O_2SO_4$ Obtained from Curve-Fitting Analysis of S K-Edge EXAFS[a]**

| | shell | CN[b] (±0.2) | $r$, Å[c] (±0.03) | $\sigma^2$,[d] $10^{-2}$ Å$^2$ (±0.002) | $R$ factor, % |
|---|---|---|---|---|---|
| $(La_{0.8}Ce_{0.2})_2O_2SO_4$, 800 °C | S−O | 4.1 | 1.48 | 0.032 | 9.9 |
| $(La_{0.8}Ce_{0.2})_2O_2SO_4$, 900 °C | S−O | 3.3 | 1.51 | 0.032 | 4.2 |
| $(La_{0.9}Ce_{0.1})_2O_2SO_4$, 800 °C | S−O | 3.4 | 1.48 | 0.032 | 7.5 |
| $(La_{0.9}Ce_{0.1})_2O_2SO_4$, 900 °C | S−O | 2.9 | 1.52 | 0.032 | 4.2 |
| $La_2O_2SO_4$ | S−O(1) | 2.0 | 1.43 | 0.032 | 2.7 |
| | S−O(2) | 2.0 | 1.47 | 0.090 | |
| $Pr_2O_2SO_4$ | S−O(1) | 2.0 | 1.43 | 0.032 | 2.5 |
| | S−O(2) | 2.0 | 1.53 | 0.063 | |

[a] Interval of $k$-space to $r$-space of FT is 3.0−13.0 Å$^{-1}$. [b] Coordination number. [c] Atomic distance. [d] Debye−Waller factor.

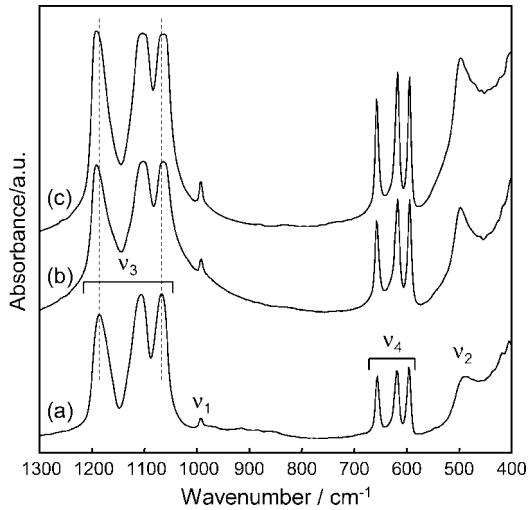


**Figure 6.** FTIR spectra of $(La_{1-x}Ce_x)_2O_2SO_4$ with (a) $x = 0$, (b) 0.1, and (c) 0.2 after calcination at 900 °C.

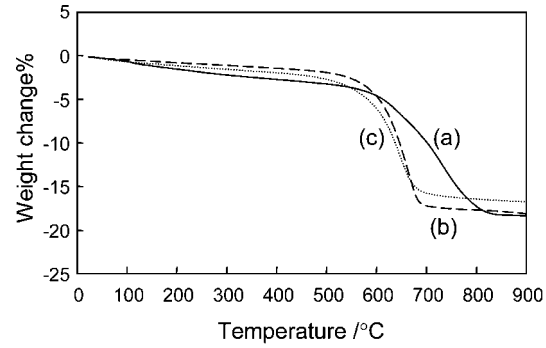


**Figure 7.** TG curves for 1 wt % Pd-loaded $(La_{1-x}Ce_x)_2O_2SO_4$ with (a) $x = 0$, (b) 0.1, and (c) 0.2 during reduction in a flow of 1.4% $H_2$/He. Heating rate: 10 °C·min$^{-1}$.

the true atomic distance. $La_2O_2SO_4$ showed a peak having a shoulder in the first neighboring shell. By contrast, no such shoulders were observed for $(La_{0.8}Ce_{0.2})_2O_2SO_4$. Table 4 shows structural parameters obtained from curve-fitting analysis of S K-edge EXAFS. The fitting results are included in the Supporting Information (Figure S1). Two references, $La_2O_2SO_4$ as well as $Pr_2O_2SO_4$, were found to have two distinct S−O atomic distances. It should be noted that $Pr_2O_2SO_4$ showed a larger difference in the S−O atomic distances (1.43 and 1.53 Å) than $La_2O_2SO_4$ (1.43 and 1.47 Å). The result indicates a higher distortion of the $SO_4$ tetrahedral unit in $Pr_2O_2SO_4$ than in $La_2O_2SO_4$, which was in accordance with our previous results on the Rietveld analysis of powder XRD profiles.[15,16] By contrast, $(La_{0.8}Ce_{0.2})_2O_2SO_4$after heating at 800 °C (a) showed a single S−O atomic distance. Because the impurity ($CeOSO_4$, see Figure 1) may affect the EXAFS spectrum, the sample after heating at 900 °C (b) was also measured, but the result still indicated a single S−O atomic distance. The coordination number of the S−O bond less than 4 was observed for the Ce-substituted compounds after heating at 900 °C, but this is not indicating the presence of $SO_3^{2-}$ as judged from S 2p XPS spectra. The reduced numbers of coordination are possibly related to the relatively large $R$ factors (Table 4).

The local structure of sulfate species was also studied by means of IR spectroscopy (Figure 6). A free $SO_4^{2-}$ ion with an ideal $T_d$ symmetry is known to show four fundamental modes; the $\nu_3$ and $\nu_4$ modes are IR active and the $\nu_1$ and $\nu_2$ modes are IR inactive.[23] Actually, however, all of these modes appears in the IR spectra because of lowering of the symmetry from $T_d$ to $C_{2v}$.[15] In addition, $\nu_3$ and $\nu_4$ each splitting into three bands suggest bridged bidentate-type coordination of $SO_4$ to La(Ce). Because the width of splitting for each mode was increased with an increase of $x$, the symmetry is supposed to be further lowered upon substitution of Ce. On the other hand, the Raman spectra of $(La_{1-x}Ce_x)_2O_2SO_4$ gave a strong single peak at approximately 990 cm$^{-1}$ due to $\nu_1$ mode, indicating the presence of a sole $SO_4$ species. With all results taken into consideration, the $SO_4$ unit of $(La_{1-x}Ce_x)_2O_2SO_4$ becomes more distorted with an increase of $x$. According to the EXAFS (Figure 5), however, the Ce-substitution rather decreased the difference of two S−O lengths in $SO_4$. Hence the structural distortion may possibly result from the O−S−O angles. Our previous work[15] suggested a positive correlation between the degree of distortion of the sulfate ion from tetrahedral and the ease of reduction of sulfate.

**Oxygen Release/Storage Property.** The oxygen release and storage properties were studied for 1 wt % Pd loaded $(La_{1-x}Ce_x)_2O_2SO_4$. Pd plays a role of the catalyst to facilitate the surface reaction with reducing gases such as $H_2$ and CO or $O_2$ in the oxygen release/storage processes.[11,12,14] To remove the impurity ($CeOSO_4$), Ce-substituted samples after heating at 800 °C and subsequent Pd loading were treated at 600 °C in a flow of 1.4% $H_2$/He and subsequently in a flow of 0.7% $O_2$/He prior to the measurement. Figure 7 shows the weight change of 1 wt % Pd loaded $(La_{1-x}Ce_x)_2O_2SO_4$ in a flow of 1.4% $H_2$/He, which was measured by the use of the flow microbalance. The oxygen release from unsubstituted $La_2O_2SO_4$ ($x = 0$) started at about

(23) Nakamoto, K. *Infrared and Raman Spectra of Inorganic and Coordination Compounds*, 4th ed.; Wiley: New York, 1986.

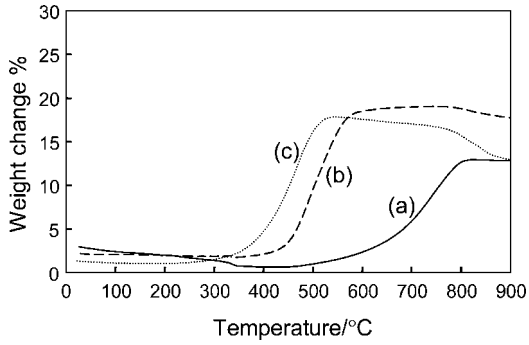


**Figure 8.** TG curves for 1 wt % Pd-loaded $(La_{1-x}Ce_x)_2O_2S$ with (a) $x = 0$, (b) 0.1, and (c) 0.2 during reoxidation in a flow of 0.7% $O_2$/He. Heating rate: 10 °C·min$^{-1}$.

600 °C and ended at about 800 °C. The weight loss (15%) is the as same as estimated from the following reduction reaction:

$$La_2O_2SO_4 + 4H_2 \rightarrow La_2O_2S + 4H_2O \quad (1)$$

Clearly, the Ce substitution increased the slope of the weight loss, which corresponds to the rate of oxygen release. At the end of each weight change in Figure 7, oxysulfates were confirmed to transform into oxysulfides, which were next subjected to the reoxidation in a flow of 0.7% $O_2$/He. Figure 8 shows the weight change of 1 wt % Pd loaded $(La_{1-x}Ce_x)_2O_2S$ due to oxygen storage during the heating. The oxygen uptake by unsubstituted $La_2O_2S$ ($x = 0$) started at ≥500 °C, but it did not complete even at about 800 °C. The total weight gain about 13% was thus lower than the calculated value (18.7%) based on the assumption of the following reoxidation.

$$La_2O_2S + 2O_2 \rightarrow La_2O_2SO_4 \quad (2)$$

As revealed in our previous work,[15] the reoxidation of $La_2O_2S$ is very slow. By contrast, the Ce substitution was found to promote significantly the oxygen uptake; that is, the onset of oxygen storage for $x = 0.2$ was observed at a low temperature of 300 °C, compared to more than 500 °C required for the unsubstituted $La_2O_2SO_4$. The observed weight gain was increased to approach to the theoretical value (≥18%). Although the increased weight gain contains the oxygen uptake due to the reoxidation of $Ce^{3+}$ to $Ce^{4+}$, its contribution should be less than 5% of the overall weight gain. Furthermore, a larger slope of the weight gain suggests the higher rate of oxygen storage. These results give the evidence that the Ce-subsitition is an efficient modification to accelerate the oxygen storage and release of the $La_2O_2SO_4$/$La_2O_2S$ system.

The oxygen storage performance was next evaluated under oscillating feed stream conditions, where reducing and oxidizing gas feeds were cycled. Figure 9 shows the weight changes of 1 wt % Pd/$(La_{1-x}Ce_x)_2O_2SO_4$ at 600 °C under a cycled feed stream condition (0.7% $O_2$ or 1.4% $H_2$, He balance). The unsubstituted $La_2O_2SO_4$ (a) showed very small and slow weight changes, which were less than 20% of theoretical OSC (2 mol-$O_2$·mol$^{-1}$) estimated from the stoichiometric reactions (eqs 1 and 2). By contrast, the Ce-substituted samples ($x = 0.1$ and 0.2) exhibited the fast and large weight changes of about 11−13%, which correspond to 70−83% of the stoichiometric reactions. During the

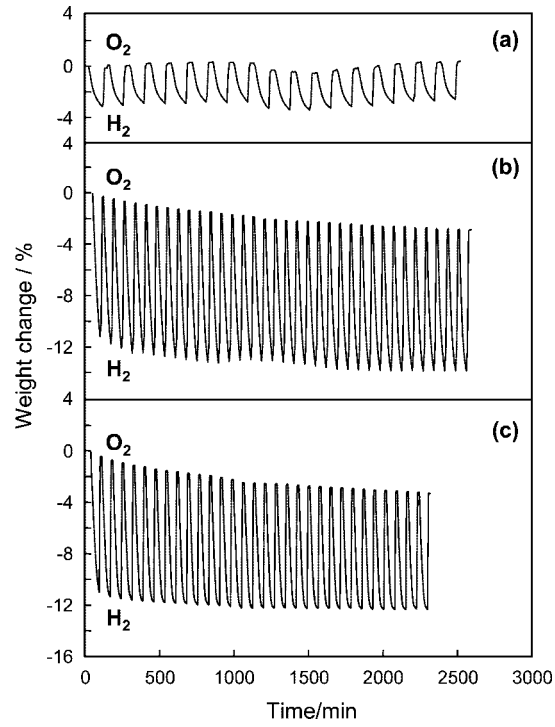


**Figure 9.** Oxygen release/storage cycles over 1 wt % Pd-loaded $(La_{1-x}Ce_x)_2O_2SO_4$ ($0 \le x \le 0.2$) at 600 °C under the cycled feed stream of 1.4% $H_2$/He and 0.7% $O_2$/He, (a) $x = 0$, (b) 0.1, and (c) 0.2.

oxygen release/storage cycles, part of Ce should alter its form between $CeO_2$ deposited on oxysulfate and $Ce^{3+}$ dissolved in oxysulfide.

The rates of oxygen release and storage were estimated from the slope of the weight change in Figure 9 and are listed in Table 5. The BET surface area of $(La_{1-x}Ce_x)_2O_2SO_4$ decreased with an increase of $x$. Nevertheless, the rates of oxygen release as well as storage of the Ce-substituted samples are more than 5 times faster than those of unsubstituted $La_2O_2SO_4$. It should also be noted that $(La_{0.8}Ce_{0.2})_2O_2SO_4$ presented the best performance, even comparable to that of $Pr_2O_2SO_4$. As was revealed in our previous work,[15] $Pr_2O_2SO_4$ can work at the lowest temperatures in a series of lanthanide oxysulfates as a result of smooth redox of $Pr^{3+}/Pr^{4+}$ on the surface and structural distortion of the $SO_4$ unit. Similarly, the $Ce^{3+}/Ce^{4+}$ species would play a role of the mediator, which promotes the redox between $SO_4^{2-}$ and $S^{2-}$. A lower symmetry of the $SO_4$ unit would also be a possible benefit for easier reduction. All the samples showed the oxygen release slower than the oxygen storage. The different rates between oxygen release and storage originate from high stability of sulfate anions toward reduction.

In the practical use of oxygen storage materials, high thermal stability under cycling redox conditions is indispensable. Although the $La_2O_2SO_4/La_2O_2S$ system is thermostable up to about 1100 °C under a static condition, gradual loss of sulfur occurs during long-term dynamic redox cycles at high temperatures of 800 °C as reported for $Pr_2O_2SO_4$ in our previous work. However, the stability could significantly be improved in the presence of a very low concentration $SO_2$, which would normally contained in a real exhaust.[14]

**Table 5. Rate of Oxygen Storage/Release for 1 wt % Pd-Loaded $(La_{1-x}Ce_x)_2O_2SO_4$ at 600 °C**

| | $x = 0$ | $x = 0.1$ | $x = 0.2$ | $Pr_2O_2SO_4$ |
|---|---|---|---|---|
| BET surface area, $m^2 \cdot g^{-1}$ | 32 | 11 | 9 | 28 |
| oxygen release, mol-$O_2 \cdot g^{-1}$ $min^{-1}$ | $0.18 \times 10^{-4}$ | $0.93 \times 10^{-4}$ | $0.85 \times 10^{-4}$ | $1.1 \times 10^{-4}$ |
| oxygen storage, mol-$O_2 \cdot g^{-1}$ $min^{-1}$ | $0.57 \times 10^{-4}$ | $3.4 \times 10^{-4}$ | $4.3 \times 10^{-4}$ | $5.4 \times 10^{-4}$ |

**Anaerobic CO Oxidation.** Finally, the Pd-loaded $(La_{1-x}Ce_x)_2O_2SO_4$ was applied to anaerobic CO oxidation at 600 °C to ensure the effect of Ce-substitution on the catalytic performance. In this experiment, two gas feeds, 1% CO and 0.5% $O_2$, were switched with intervals of 10 and 20 min, respectively. The amount of both CO and $O_2$ supplied per cycle was 1.1 mmol$\cdot g^{-1}$. Compared to the full OSC of 2 mol-$O_2 \cdot$(mol-S)$^{-1}$ = 4.9 mmol-$O_2 \cdot g^{-1}$, the interval set here is very short and corresponds to about 20% OSC. Figure 10a illustrates the typical gas concentration profiles at the inlet as well as the outlet of the catalyst bed when 1 wt % Pd/$La_2O_2SO_4$ was used at 600 °C. The $O_2$-to-CO switch yielded a temporal $CO_2$ peak with simultaneous consumption of CO, presumably suggesting the CO oxidation by PdO species. Soon after this, however, the $CO_2$ concentration declined rapidly because the oxygen release from $La_2O_2SO_4$ is slow at this temperature. The subsequent CO-to-$O_2$ switch gave rise to a very small $O_2$ uptake by the reoxidation of Pd and $La_2O_2S$, which is indicated as "OS" in the figure. The total conversion of anaerobic CO oxidation was thus less than 10%.

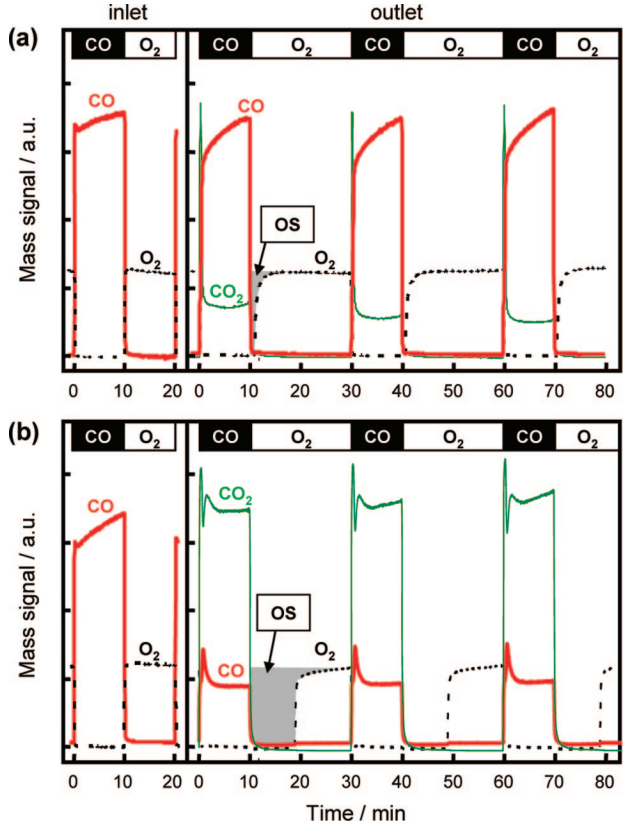


**Figure 10.** Gas concentration profiles during $CO/O_2$ cyclic reactions over (a) 1 wt % Pd-loaded $La_2O_2SO_4$ and (b) 1 wt % Pd-loaded $(La_{0.8}Ce_{0.2})_2O_2SO_4$ under cycled feed stream of 0.5% $O_2$/He and 1% CO/He at 600 °C. $W/F = 4 \times 10^{-3}$ g$\cdot$min$\cdot$cm$^{-3}$.

Compared to the Pd-loaded $La_2O_2SO_4$, the Pd-loaded $(La_{0.8}Ce_{0.2})_2O_2SO_4$ exhibited very different concentration profiles as shown in Figure 10b. After initial decay at the beginning of each CO step, almost constant CO conversion of more than 70% was obtained. The following CO-to-$O_2$ switch yielded the $O_2$ storage. The OSC calculated from the oxygen breakthrough curve achieved a much larger value of 0.43 mmol-$O_2 \cdot g^{-1}$. The observed OSC and the amount of CO converted (0.85 mmol-CO$\cdot g^{-1}$) indicates the occurrence of stoichiometric CO oxidation to $CO_2$ under the anaerobic condition, which is ascribed to the following two reactions:

$$La_2O_2SO_4 + 4CO = La_2O_2S + 4CO_2$$

$$La_2O_2S + 2O_2 = La_2O_2SO_4$$

On the basis of the above results, it can be concluded that the catalytic activity of $La_2O_2SO_4$ for oxidation of CO has been significantly improved by introducing Ce. The structural modification be mean of Ce substitution is expected to be a useful strategy for the development of large capacity oxygen storage materials.

## Conclusion

The Ce-substituted La oxysulfates, $(La_{1-x}Ce_x)_2O_2SO_4$ ($0 \le x \le 0.2$), were synthesized by a template assisted route using dodecyl sulfate ions (DS). Part of Ce in the calcined product occupied the La site in oxysulfate, but the other part was deposited as $CeOSO_4$ and/or $CeO_2$. After reduction in $H_2$, however, almost all the Ce appears to be incorporated in the oxysulfide phase. Thanks to the redox property of $Ce^{3+}/Ce^{4+}$ and possible structural distortion of $SO_4$, the Ce-substituted phase achieved the higher rates of oxygen release and storage comparable to those of $Pr_2O_2SO_4$ in our previous work. The anaerobic oxidation of CO over Pd loaded $(La_{1-x}Ce_x)_2O_2SO_4$ could be achieved at a lower temperature of 600 °C under the unsteady cycled feed stream conditions, where the unsubstituted $La_2O_2SO_4$ could not work.

**Acknowledgment.** This study was partly supported by Industrial Technology Research Grant Program from NEDO and a Grant-in-Aid for Scientific Research on Priority Area (440) from MEXT. The X-ray absorption experiments were performed at PF-KEK (Proposal No. 2006G360) with helpful advice from Dr. Y. Kitajima.

**Supporting Information Available:** $k^3$-weighted K-edge EXAFS of $(La_{0.8}Ce_{0.2})_2O_2SO_4$ (PDF). This material is available free of charge via the Internet at http://pubs.acs.org.

CM801629B